Applied Catalysis B: Environmental 219 (2017) 353–361

Contents lists available at ScienceDirect

Applied Catalysis B: Environmental

journal homepage: www.elsevier.com/locate/apcatb

Visible-light-driven photocatalytic system based on a nickel complex over CdS materials for hydrogen production from water

Qiu-Xia Peng [a], Dan Xue [a], Shu-Zhong Zhan [a,*], Chun-Lin Ni [b,*]

[a] College of Chemistry & Chemical Engineering, South China University of Technology, Guangzhou 510640, China
[b] College of Materials and Energy, Institute of Biomaterial, South China Agricultural University, Guangzhou 510642, China

ARTICLE INFO

Article history:
Received 5 May 2017
Received in revised form 7 July 2017
Accepted 12 July 2017
Available online 19 July 2017

Keywords:
Nickel complex
CdS NRs
Electrocatalytic system
Photocatalytic system
Hydrogen evolution

ABSTRACT

Based on that the evolution of renewable H_2 by using a photochemical method requires photoinduced electron transfer (ET) from a light harvester to an electrocatalyst in water, we present a nickel complex, $[BzPyN(CH_3)_2]_2[Ni(i\text{-}mnt)_2]$ **1** (i-mnt^{2-} = 2,2-dicyanoethylene-1,1-dithiolate) that acts as both an electrocatalyst and a photocatalyst for H_2 generation from water via an unstable nickel hydride intermediate. As an electrocatalyst, this nickel complex can catalyze hydrogen generation from a neutral buffer with a turnover frequency (TOF) of 577.4 mol of hydrogen per mole of catalyst per hour (mol H_2/mol catalyst/h) at an overpotential (OP) of 837.6 mV. As a photocatalyst, combining with CdS nanorods (CdS NRs) as a photosensitizer, and ascorbic acid (H_2A) as a sacrificial electron donor, it can photocatalyze hydrogen evolution in heterogeneous environments and can work for 100 h. Under an optimal condition, the highest hydrogen evolution turnover number (TON) reaches 85820 mol of H_2 per mol of catalyst during 70 h irradiation, and the highest apparent quantum yield (AQY) is ~23% at 420 nm. And possible cycles for H_2 production by the electrocatalytic and photocatalytic systems are afforded.

1. Introduction

To suppress the growth of CO_2 emissions and its consequent effects on global climate change, many synthetic systems have been developed with the hope of employing natural resources to get renewable energy, such as hydrogen. Hydrogen is one ideal energy in the future, because of its recyclability and pollution-free use. Water reduction is an important method for hydrogen production, which can be used as a cheap, green fuel [1–3]. In particular, electro- and photo-catalytic methods for generating hydrogen from water have been explored as cost-effective ways of producing a carbon-neutral fuel. The most viable method for large-scale growth in carbon-free energy is the light-driven splitting of water into its constituent elements [4–6]. Now, the key issue on the splitting of water is the design of an efficient system for water reduction to hydrogen with high turnover rates, good stability and durability [7,8]. As we know, hydrogenase enzymes, containing transition metal complexes (such as iron and nickel) can efficiently catalyze both the production and the oxidation of hydrogen [9,10]. As the stability is often limited outside of their native environment, it is impossible to get in large amounts for practical uses [9,10]. To mimic the performance of this natural process, large effort has been focused on the design and development of molecular catalysts for photochemical driven water reduction to hydrogen, and several complexes that contain nickel [11–13], cobalt [14–16] and iron [17] have been designed as photo-catalysts for the reduction of water to form H_2. In a typical system, these molecular catalysts are combined with a molecular photosensitizer (PS), such as ruthenium(II) trisbipyridyl complex, $Ru(bpy)_3Cl_2$ and a sacrificial electron donor. However, these photosensitizers can suffer degradation during irradiation [18–20].

Inspired by Honda's work that photocatalytic splitting of water occurs on TiO_2 electrodes [21], photocatalysis has demonstrated wide ranging potential applications in areas such as converting solar energy. To mimic natural photosynthesis by converting solar energy into chemical energy, the research on the photocatalytic splitting of water to produce hydrogen, has been carried out extensively [22–25]. Considering that the visible light accounts for about 43% of the solar radiation energy, while the ultraviolet light only contributes to about 4%, people have been focusing on the design of visible-light-responsive photocatalysts [26–29].

At present, CdS materials are selected as photosensitizers for the conversion of solar energy into chemical energy under visible-light irradiation, because CdS has a narrow band gap (with an Eg of 2.4 eV). Moreover, the potential of its conduction band (CB) is more

* Corresponding authors.
E-mail addresses: shzhzhan@scut.edu.cn (S.-Z. Zhan), niclchem@scau.edu.cn (C.-L. Ni).

http://dx.doi.org/10.1016/j.apcatb.2017.07.034
0926-3373/

negative than the reduction potential of hydrogen proton (H^+/H_2), letting it more proper for the H_2 generation [30–33]. However, the photocatalytic activity of CdS itself toward water reduction is very low due to high-rate charge recombination of photogenerated electron [34]. In order to suppress this recombination, the design of a cocatalyst, which can be loaded on CdS is an ideal method for improving the photocatalytic activity [35–39]. Generally, noble metals, such as Pt, Pd and Rh are proper candidates, because they can attract and trap photo-electrons and suppress the recombination of electron-hole pairs, which together improve the efficiency of electron utilization. However, noble metals are very expensive, it is necessary to develop non-noble-metal catalysts [37]. These considerations have led to the development of cocatalysts employing more abundant metals, and several transition metal complexes have been developed as cocatalysts for the production of hydrogen [40,41]. In this paper, we report a catalyst based on the nickel complex, $[BzPyN(CH_3)_2]_2[Ni(i\text{-}mnt)_2]$ **1**. This nickel complex can serve as a low-cost and efficient cocatalyst for H_2 production in an artificial photocatalytic system combining CdS NRs as a photosensitizer, and ascorbic acid (H_2A) as a sacrificial electron donor.

2. Experimental

According to the reported methods, 1-(4′-chlorobenzyl)-4-dimethylaminopyridinium bromide ($[4ClBzPyN(CH_3)_2]Br$) and disodium maleonitriledithiolate (Na_2mnt) were synthesized [42]. $[BzPyN(CH_3)_2]_2[Ni(i\text{-}mnt)_2]$ **1** ($i\text{-}mnt^{2-}$ = iso-maleonitriledithiolate) was prepared according to the literature procedures [43]. The CdS nanorods (CdS NRs) was prepared by using the reported method [44]. Physical measurements for electrochemical analysis can be found in the supported information. A Hitachi U-3010 spectrometer was used to measure UV–vis spectra. The luminescent spectra were recorded on a F-4500 fluorescence spectrophotometer. The energy dispersive spectrometer (EDS) measurement was carried out on a Shimadzu EPMA-1600 electron probe X-ray microanalyser. The electrochemical impedance spectra (EIS) measurements were performed in the presence of a 0.010 M $K_3[Fe(CN)_6]/K_4[Fe(CN)_6]$ (1:1) mixture as a redox probe in 0.1 M KCl solution. For the photocatalytic system, each sample was prepared in a flask of buffer solution with ascorbic acid, CdS, and the nickel complex. Then, the flask was sealed with a septum. At room temperature, blue light (469 nm) was used to irradiate each sample. After photocatalysis, a 0.50 mL aliquot of the headspace was removed and replaced with 0.50 mL of CH_4. The headspace sample was injected into the gas chromatograph (GC). An Agilent Technologies 7890A gas chromatography instrument was used for GC experiments. Measurements and analysis for the chemical compositions and valence states of the photocatalysts were carried out by ESCALAB 250 Xi X-photoelectron spectroscopy (XPS) with monochromatic Al Kα (1486.6 eV) X-ray sources. Transmission Electron Microscopy (TEM) images were afforded by using a JEM-2010 electron microscope. Scanning electron microscopy (SEM) images were obtained on a Merlin emission gun SEM instrument. Measurements and analysis for the crystalline diffraction patterns of CdS NRs and the related components were carried out by using Bruker D8 Advance powder X-ray diffraction.

3. Results and discussion

3.1. Electrocatalytic system based on complex *1* for hydrogen evolution

The reaction of $NiCl_2{\cdot}6H_2O$, $Na_2(i\text{-}mnt)$ and 1-benzyl-4-(dimethylamino)pyridinium ($[BzPyN(CH_3)_2]$) affords a nickel(II) complex, $[BzPyN(CH_3)_2]_2[Ni(i\text{-}mnt)_2]$ **1** (Scheme 1) [43]. It has

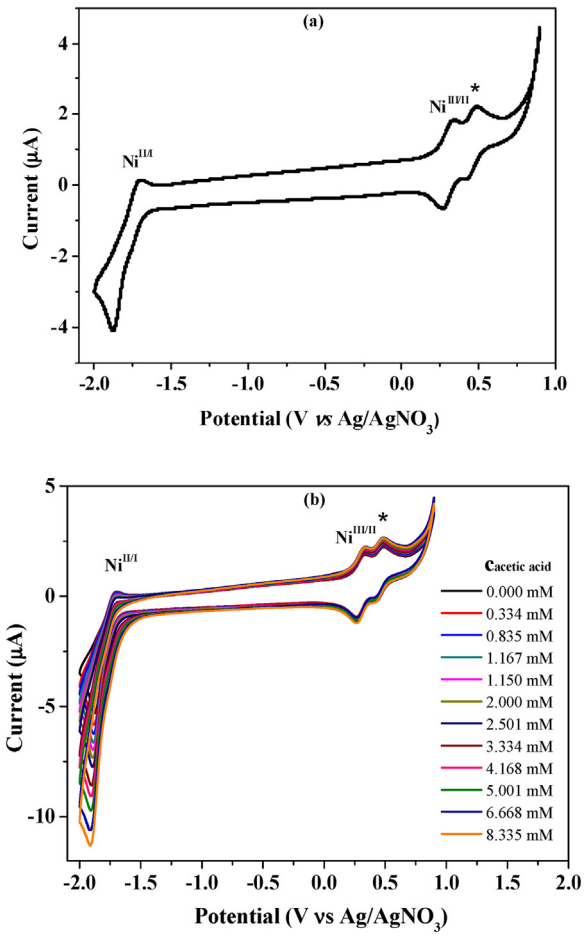

Fig. 1. (a) Cyclic voltammograms (CVs) of 0.30 mM complex **1** in DMF with 0.10 M of $[n\text{-}Bu_4N]ClO_4$. (b) CVs of a 0.30 mM of complex **1** in DMF with varying concentrations of acetic acid. Conditions: Glassy carbon working electrode (1.0 mm diameter), Pt counter electrode, $Ag/AgNO_3$ reference electrode, scan rate 100 mV/s. Ferrocene internal standard (*).

shown that nickel complex can electrocatalyze hydrogen generation via an unstable hydride intermediate [45], first we checked if this nickel complex also can act as an electrocatalyst for hydrogen generation in homogeneous environments. In DMF solution, complex **1** displayed two reversible waves at 0.30 and −1.79 V versus $Ag/AgNO_3$, which are assigned to the couples of $Ni^{III/II}$ and $Ni^{II/I}$, respectively (Fig. 1a). According to Fig. S1, no significant change is found after several scans, indicating that this nickel complex is stable under these conditions.

As a rule, organic acid such as acetic acid is used as proton resource to test the electrocatalytic performance of the designed electrocatalysts. As shown in Fig. 1b, with the addition of varied content of acetic acid (from 0.0 to 8.335 mM), voltammetric currents emerging at −1.88 V increase. Note, the position of this peak is independent of the acid concentration and corresponds to a one-electron reduction of the protonated complex to **1-H** [46]. Moreover, the current strengths at −1.88 V decrease with the addition of triethylamine (TEA) (Fig. S2). This can be attributed to the neutralization of hydrogen proton in **1-H** by TEA. This finding indicates that the reduction of Ni(II) to Ni(I) and protonation are responsible for hydrogen generation in the above electrocatalytic system.

In light of the above observations, analyses and literature precedent [47], an electrocatalytic cycle for proton reduction to hydrogen is put forward. From Scheme 2, the nickel(I) species, $[Ni^{I}(i\text{-}mnt)_2]^{3-}$ is obtained by one-electron reduction of $[Ni^{II}(i\text{-}mnt)_2]^{2-}$ **1**. Then

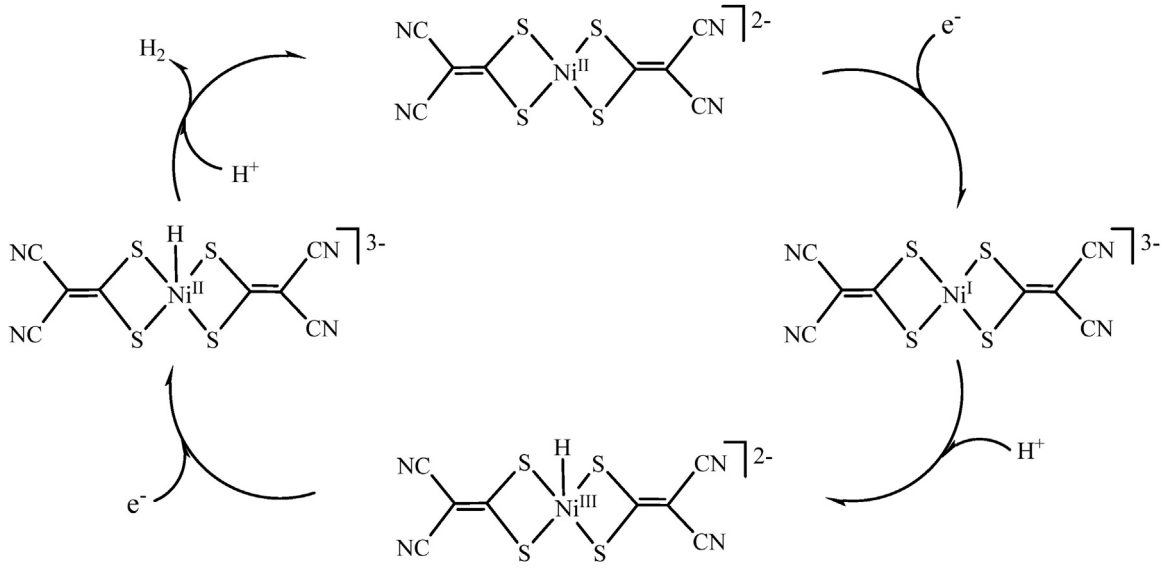

Scheme 1. Synthesis of the nickel complex, $[BzPyN(CH_3)_2]_2[Ni(i\text{-}mnt)_2]$ **1**.

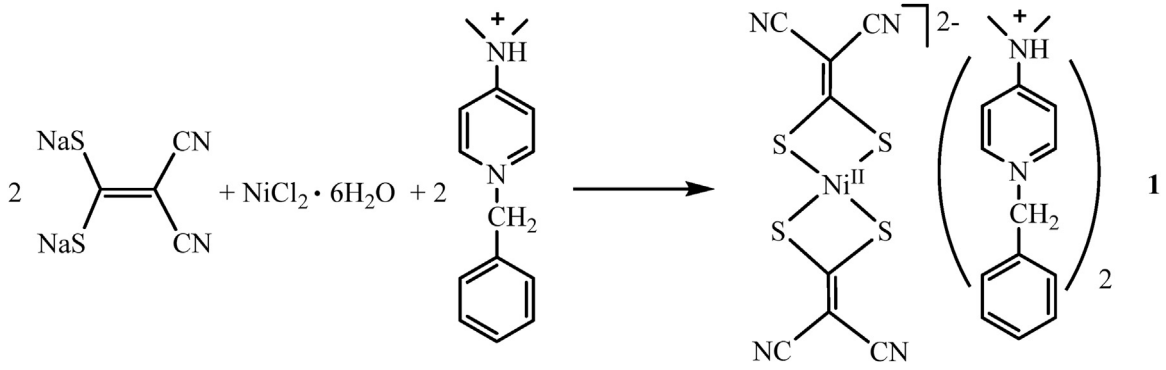

Scheme 2. A possible electrocatalytic mechanism for proton reduction to hydrogen by $[BzPyN(CH_3)_2]_2[Ni(i\text{-}mnt)_2]$ **1**.

the introduction of hydrogen proton (H^+) results in one Ni^{III}-H species, $[H\text{-}Ni^{III}(i\text{-}mnt)_2]^{2-}$. Another one-electron reduction of the Ni^{III}-H species leads to the formation of the Ni^{II}-H species, $[H\text{-}Ni^{II}(i\text{-}mnt)_2]^{3-}$. Dihydrogen is afforded by further introduction of hydrogen proton (H^+), and the starting sample is regenerated.

Then, bulk electrolysis was employed to characterize the electrocatalytic activity of complex **1** and results were showed in Fig. S3a. For example, with the introduction of complex **1**, the electrocatalytic system affords 80 mC of charge during 2 min of electrolysis under −1.45 V versus $Ag/AgNO_3$, with accompanying production of a gas. Gas chromatography (GC) was used to detect the H_2 produced after a 2 h bulk electrolysis (Fig. S4). According to Fig. S3b, a CPE experiment under same conditions without complex **1** only gives a charge of 3 mC. These results indicate that this nickel complex does indeed serve as an electrocatalyst for hydrogen production. The overpotential (OP) and turnover frequency (TOF) were calculated by using Evans's method, Eq. (1) [48], and Eq. (2) [49], respectively, and results were listed in Fig. S5.

Overpotential = Applied potential $-E^{\circ}_{HA}$

$$= \text{Appliedpotential} - (E^{\circ}{}_{H^+}\text{-}(2.303RT/F)pK_{aHA}) \quad (1)$$

$$\text{TOF} = \Delta C/(F{*}n_1{*}n_2{*}t) \quad (2)$$

Where, F is Faraday's constant, n_1 is the number of moles of electrons required to generate one mole of H_2, n_2 is the number of moles of catalyst in solution, and t is the duration of electrolysis; ΔC is the charge from the catalyst solution minus the charge from solution without catalyst.

After that we examined the electrocatalytic function in aqueous media. According to Fig. S6, in the presence of **1**, with decreasing pH values from 7.0 to 2.7, the strength of the reduction wave increases and the onset of the catalytic wave are shifted to higher potentials, which are assigned to a catalytic process [50]. Note, at pH 7.0, complex **1** exhibits one quasi-reversible redox wave at −0.24 versus Ag/AgCl (Fig. S6-inset), which is assigned to the Ni^{II}/Ni^{I} couple.

Further characterization for the electrocatalytic activity of complex **1** in aqueous media came from bulk electrolysis in buffer and the total charge of bulk electrolysis from a neutral buffer (pH 7.0) with and without **1** were plotted in Fig. S7. For instance, under −1.45 V versus Ag/AgCl, this buffer solution provides only 20 mC during 2 min of electrolysis in the absence of **1** (Fig. S7a). Surprisingly, the introduction of **1** results in 1014 mC of charge under identical conditions (Fig. S7b) and a large number of gas bubbles, which are confirmed to be H_2 by GC. The data listed in Fig. S8a show that this nickel complex can afford 3.96 mL of H_2 during a 1 h electrolysis with a Faradaic efficiency of 92% (Fig. S8b). Based on Eqs. (2) and (3) [51], TOFs for electrocatalytic hydrogen production by complex **1** are calculated (Eq. S2), and results are listed in Fig. S9. For example, this electrocatalytic system can afford 577.4 mol of hydrogen per mole of catalyst per hour at an OP of 837.6 mV.

$$\text{Overpotential} = \text{Applied potential-E(pH)} = \text{Applied potential-}(-0.059\,\text{pH}) \quad (3)$$

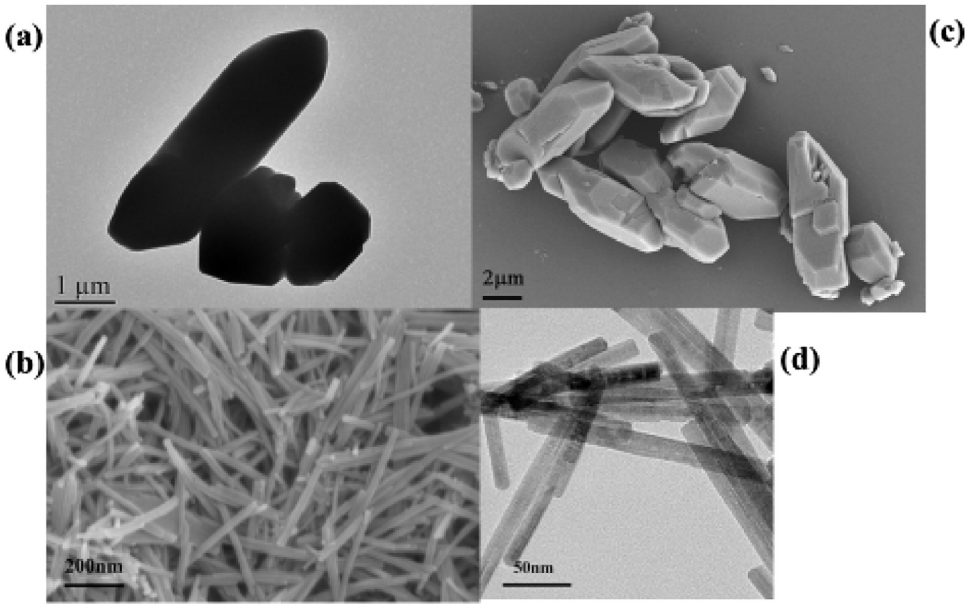

Fig. 2. (a) TEM image of complex **1**. (b) SEM image of CdS nanorods (CdS NRs). (c) SEM images of complex **1**. (d) TEM images of CdS NRs.

3.2. Investigation for the stability and durability of complex *1* in the electrocatalytic system

In order to test whether complex **1** retains its activity over longer time, a 72 h CPE under −1.45 V versus Ag/AgCl was conducted in a neutral 0.25 M buffer solution (pH 7.0) containing 6.5 μM of complex **1**. From Fig. S10, the catalytic current remains almost constant over an electrolysis period of 72 h, indicating that this nickel complex is stable in the above electrocatalytic system. After this period, the pH had increased by 5.3 units (from 7.0 to 12.3), consistent with accumulation of OH^- by water reduction, $2H_2O + 2e \rightarrow H_2 + 2OH^-$. Note, the original electrocatalytic function was recovered and this experiment could be repeated several times when the solution pH was adjusted back to the original value of 7.0, indicating that this nickel-based catalyst can be reused. Then UV–vis spectra were used to test the stability of complex **1** by employing an optically semi-transparent thin layer electrode. As shown in Fig. S11, the electrochemical reduction of complex **1** at −1.45 V versus Ag/AgCl results in no new absorption waves over an electrolysis period of 72 h, and the intensities of the absorption bands at 291, 342, 455 nm are almost the same, indicating this nickel complex is stable under these conditions. Moreover, this result is supported by the electrochemical measurements that the catalytic current does not change over a 20-cycle CVs (Fig. S1), which always be considered as the formation of a catalytic deposits [52]. The above result is also in agreement with the following energy dispersive spectrometer (EDS) analysis. From Fig. S12, after 6 h electrolysis, there is no evidence for the formation of precipitate on the glassy carbon electrode by EDS.

3.3. Photocatalytic system for H_2 generation

Based on the above electrocatalytic investigations, we examined the photocatalytic performance of the heterogeneous system containing complex **1** (Fig. 2a and c) as a cocatalyst, ascorbic acid (H_2A) as an electron donor and CdS NRs (Fig. 2b and d) as a photosensitizer. In accordance with the general rules, a series of photolysis experiments were carried out with varying pH values to investigate the effect of pH of media on the activity of H_2 production. According to the data plotted in Fig. S13, the best pH for photocatalytic H_2 generation mediated by **1** (0.02 mM) is observed at pH 3.7, with a TON of 3989 mol of H_2 (mol of cat)$^{-1}$ during 2 h of irradiation.

To get an optimal photocatalytic system, several measurements were carried out in parallel for comparison. First we checked the effect of the concentrations of sacrificial reagent and photosensitizer on the photocatalytic H_2 generation catalyzed by complex **1**. For instance, to a photocatalytic system containing 0.12 M ascorbic acid, 0.010 mM complex **1** and a varying content of CdS NRs, the TON during 2 h of photolysis increases with increasing the concentration of CdS NRs until a saturation value of 4423 mol of H_2 (mol of cat)$^{-1}$ is reached at 0.090 mL^{-1}. Then, the TON decreases when the concentration of CdS NRs is set to more (Fig. S14). Other photocatalytic systems containing 0.05 mg mL^{-1} CdS, 0.02 mM complex **1** and varying contents of ascorbic acid were designed to select the best ratio of ascorbic acid. According to Fig. S15, the TON used in 2 h increases with increasing the concentration of ascorbic acid until a highest value of 4201 mol of H_2 (mol of cat)$^{-1}$ is reached at 0.12 M. Then, the TON decreases when the concentrations of ascorbic acid is set to more.

To characterize the effect of photocatalyst concentration on hydrogen production, a series of 3 h photolysis experiments were carried out with varying concentrations of complex **1**. According to Fig. S16, under continuous irradiation, **1** photocatalyzes H_2 production with a TON of 4347 mol of H_2 (mol of cat)$^{-1}$ at 0.05 mM. When the concentration of **1** is lowered to 0.01 mM, the TON increases significantly to 9078 mol of H_2 (mol of cat)$^{-1}$ (Fig. S16), showing that the concentration of **1** has a significant effect on the photocatalytic activity for H_2 production. The dependence of TON on the catalyst concentration indicates that the formation of polynuclear species might be involved in the inactivation of complex **1** [53]. And the protonation of the Ni(I) species which is more favored at lower concentration.

The above observation and analysis result in an optimal three-component system, containing 0.09 mg mL^{-1} CdS NRs, 0.12 M ascorbic acid, and 0.02 mM complex **1**. According to the data plotted in Fig. 3, H_2 generation starts immediately upon light irradiation of this system and their rates increase sharply and can last for about 70 h. Then the hydrogen generation build-up slightly increases until H_2 formation ceased after about 100 h. This system can photocat-

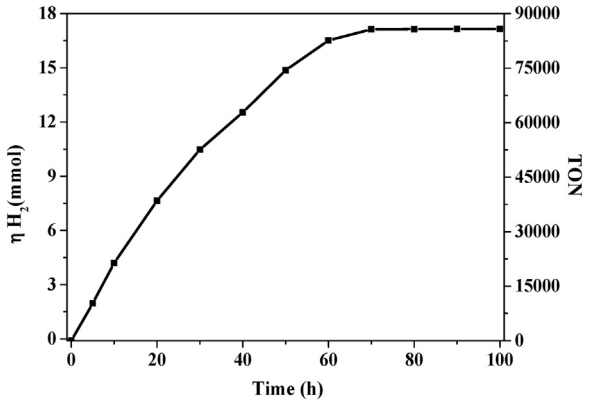

Fig. 3. Hydrogen evolution kinetics obtained upon continuous visible irradiation (λ = 469 nm) of a pH 3.7 buffer solution containing 0.09 mg mL^{-1} CdS, 0.12 M ascorbic acid, and 0.02 mM complex **1**.

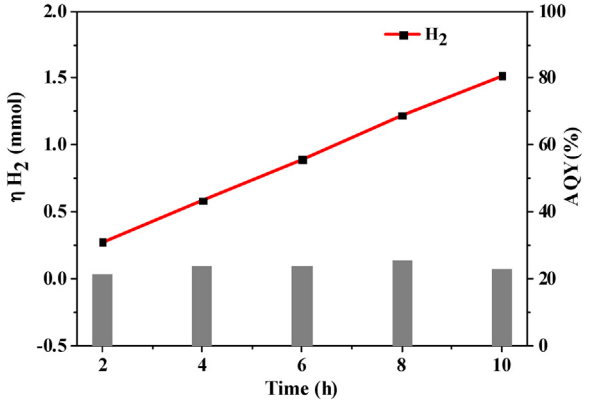

Fig. 4. Photocatalytic H_2 production of complex **1** under visible light (λ = 569 nm) and an apparent quantum yield (AQY) of complex **1** under monochromatic light (λ = 420 nm). The reaction system contained 0.090 mg CdS NRs, 0.020 mM complex **1**, 0.12 M ascorbic acid (pH 3.7).

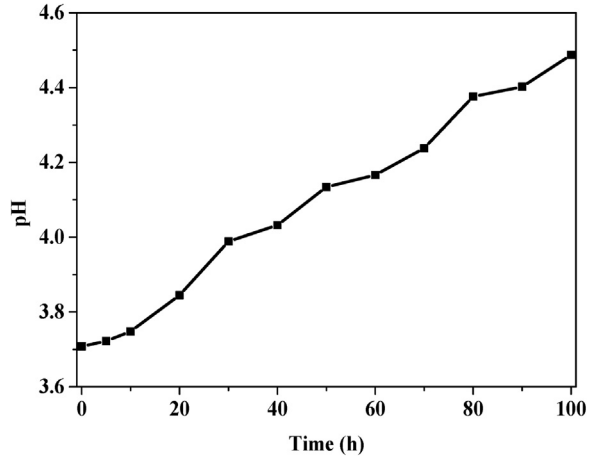

Fig. 5. pH values change of the catalytic system (0.12 M ascorbic acid, 0.09 mg mL^{-1} CdS NRs and 0.02 mM complex **1**) during photolysis.

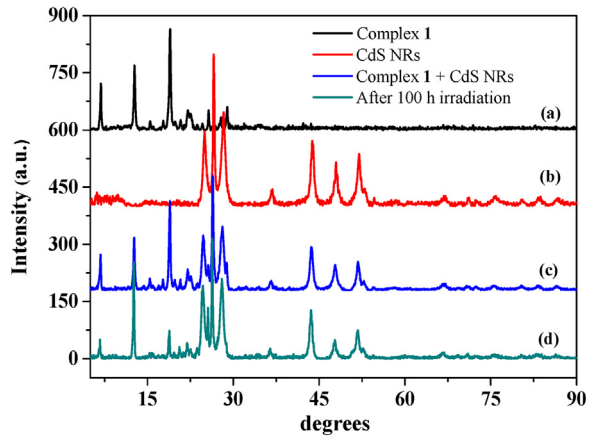

Fig. 6. XRD patterns of CdS NRs, complex **1** and the CdS NRs–**1** composite photocatalysts (before and after irradiation).

alyze H_2 production over 70 h and achieve a turnover number (TON) of 85820 mol of H_2 per mol of catalyst.

To know the apparent quantum yields (AQYs), the photocatalytic system was irradiated for 10 h under monochromic light with a band-pass filter (λ = 420 nm + 5 nm). According to Eq. (4) [54], the AQYs of the photocatalytic system for H_2 generation are calculated and results are listed in Fig. 4. Initially, the AQY is ~21% in the first 2 h. After the first 2 h, the AQYs increase. The average value of AQY is calculated to be ~23% after 10 h of irradiation.

$$AQY(\%) = (2 \cdot n_{H2} \cdot N_A \cdot h \cdot c)/(t_{irr} \cdot \lambda \cdot I \cdot A) \cdot 100 \quad (4)$$

n_{H2} is the hydrogen generation (mol H_2), N_A is the Avogadro constant, h is the Planck constant, c is speed of light, t_{irr} is the irradiation time, I is the intensity, A is the irradiated area of the photoreactor, where, I is 5 mW cm^{-2}, A is 19.63 cm^2, t_{irr} is 7200s.

To identify factors responsible for the photocatalytic H_2 evolution in the above system, we added any two of the three components (ascorbic acid, CdS NRs, or complex **1**) to a reaction flask to see if the H_2 production can be formed. According to Fig. S17, a mixture of complex **1** and CdS NRs only affords 0.64 μmol H_2, the integration of ascorbic acid and CdS NRs leads to an increase in H_2 evolution (2.5 μmol), and 1.0 μmol H_2 is produced when ascorbic acid and complex **1** is combined. Thus, the composition of the nickel complex, ascorbic acid and CdS NRs is essential for the photocatalytic activity in this reaction system.

To test the effect of the (crystallinity) morphology of CdS on the catalytic activity, we also investigated the photocatalytic systems with CdS clusters (Fig. S18) and CdS NRs (Fig. 2b), respectively. As shown in Figs. S19,S20, CdS NR exhibits much better photocatalytic performance than that of CdS cluster. This can be attributed to nanosize effects that the smaller size caused larger surface area and thus more catalytic sites.

3.4. Investigation for the stability and durability of the photocatalytic system

The stability of the catalytic system under turnover conditions is a general concern. As shown in Fig. 5, after a 100 h photolysis period, the pH had increased by 0.8 units (from 3.7 to 4.5), consistent with accumulation of OH^- by water reduction, $2H_2O + 2e \rightarrow H_2 + 2OH^-$. However, this catalytic function could be recovered in 43% when the solution pH was adjusted back to the original 3.7. This result can be attributed to the decomposition of CdS NRs, ascorbic acid or complex **1** during photolysis.

To answer these equations, several physical or physiochemical methods were employed for measurements and analysis. First, we employed powder X-ray diffraction (XRD) technology to characterize this photocatalytic system. After 100 h irradiation, the mixture of complex **1** and CdS NRs was washed by CH_3CN and water, respectively, then investigated by using XRD methods. The XRD data of the related components were listed in Fig. 6a–d. Fig. 6c shows the XRD pattern of complex **1**/CdS NRs composite (blue), in which all the different peaks are also well matched with the pattern of CdS

NRs (Fig. 6b), indicating that the introduction of the nickel complex does not affect the crystallinity of CdS NRs. According to Fig. 6d, the XRD signs are same as those before irradiation, indicating that both CdS NRs and complex **1** are stable during 100 h of photolysis.

For photocatalytic H_2 production systems composited by metal compounds, one may wonder if these compounds actually decomposed to form metal as the real catalyst for proton reduction. To identify the chemical composition and oxidation state of different atoms in the composite particles before and after irradiation, the X-ray photoelectron spectroscopy (XPS) of the photocatalyst samples were measured. As shown in Fig. 7a, the black plot is the spectrum of a mixed complex **1**/CdS NR sample and the red plot is for the sample washed by acetonitrile and water after 100 h photocatalysis. Both survey spectra are quite similar, with the presence of Cd, S, O, and C elements. Before photocatalysis, the high resolution XPS spectra of S 2p and Cd 3d are exhibited in Fig. 7b and c. Two main peaks are located at 162.68 and 161.44 eV, which can be attributed to S 2p in CdS NRs [55–57]. Fig. 7c demonstrates two obvious Cd 3d peaks located at 404.95 eV and 411.70 eV, which are consistent with the Cd character in CdS NRs [55].

After 100 h irradiation, the position or strength of both S 2 s and Cd 3d peaks remain almost constant, indicating that CdS NRs is stable as a photosensitizer during photocatalysis. The high resolution

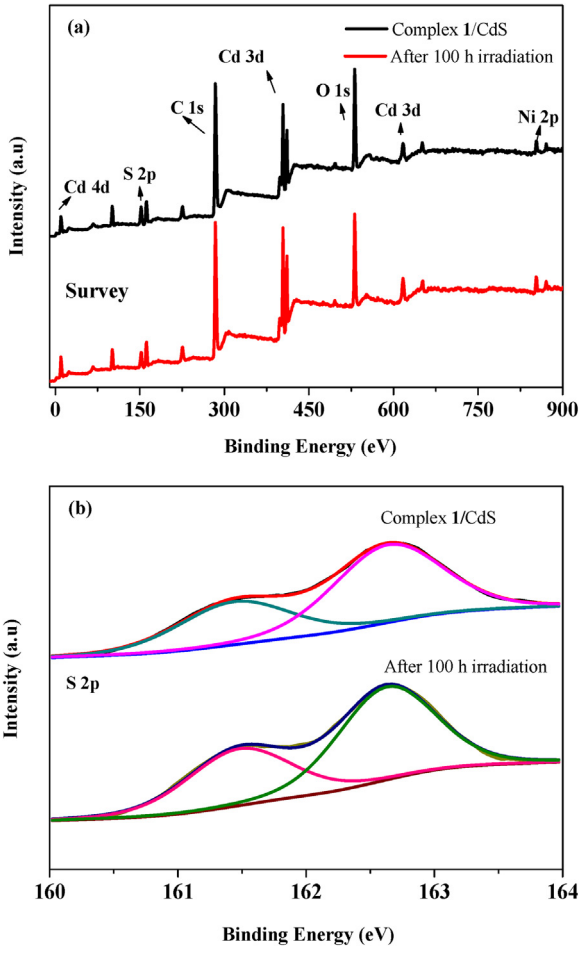

Fig. 7. (a) XPS survey spectra of the photocatalyst samples. The black plot is for the mixture of CdS NRs and complex **1**. The red plot is the photocatalyst after the H_2 production reaction, which was centrifuged and washed by acetonitrile and water after 100 h of irradiation. (b) High resolution spectra of S 2p peaks at 161.32 eV and 162.53 eV. (c) High resolution spectra of Cd 3d peaks at 405.02 eV and 411.69 eV. (d) High resolution spectra of Ni 2p peaks at 854.78 eV and 871.781 eV (For interpretation of the references to colour in this figure legend, the reader is referred to the web version of this article.)

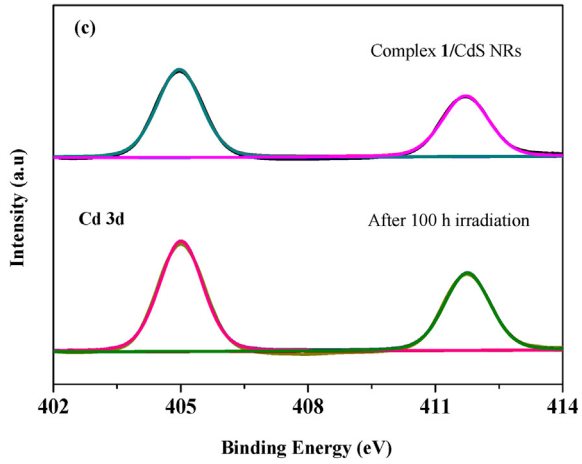

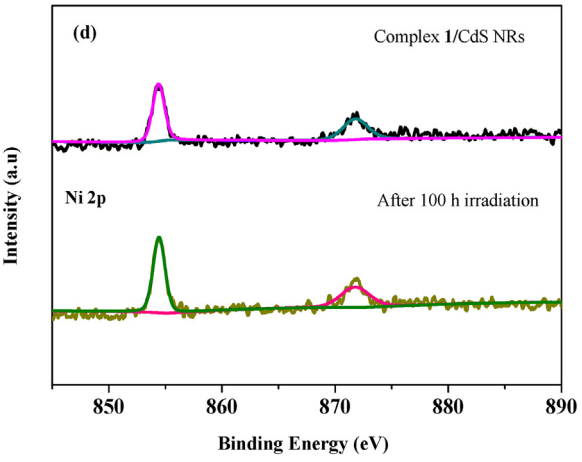

Fig. 7. (*Continued*)

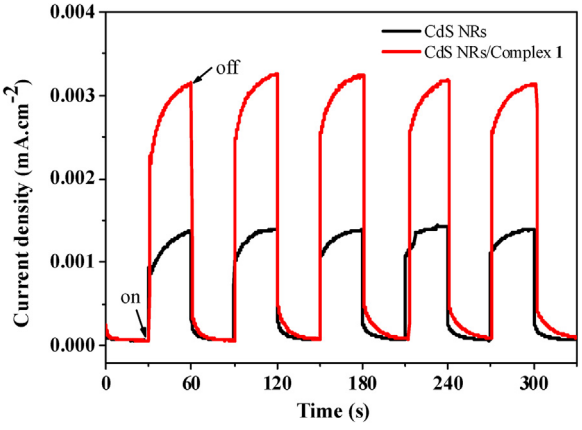

Fig. 8. Current responses versus time of the nickel complex/CdS NRs under visible-light irradiation (λ > 420 nm) at 0.0 V using Ag/AgCl as a reference electrode.

XPS spectrum of Ni 2p in a mixed complex **1**/CdS NRs sample is shown in Fig. 7d. Before irradiation, two appreciable Ni 2p peaks are observed at 854.78 eV and 871.781 eV, indicating the presence of a Ni^{2+} ion. In contrast, no apparent Ni 2p peaks can be seen in the sample after irradiation, further confirming no metallic nickel formation during photocatalytic H_2 production over a period of 100 h photocatalysis. Moreover, Fig. 8 shows the photocurrent response versus time of the nickel complex/CdS NRs and CdS NRs, respectively. It is found that the photocurrent response of the nickel complex/CdS NRs is fairly reversible and stable, as shown in Fig. 8,

from which we can see that the current can reproducibly increase violently under each irradiation and recover rapidly in the dark.

From Fig. S21, before irradiation, the three-component system affords a main peak at 259 nm, which is assigned to that of ascorbic acid alone. According to Fig. S22, the photochemical reduction catalyzed by **1** results in no new absorption, and the strength of peak at 259 nm decreases over a photolysis period of 100 h, indicating that the amount of ascorbic acid decreases after photolysis under visible light. However, after 100 h photolysis, the adjustment of H_2A back to the original 0.12 M resumes nearly 53% activity of the photocatalytic system under another illumination. Following, when the solution pH was adjusted back to the original value of 3.7, the original photocatalytic function was recovered about 93%. These results indicate that although some components of the photocatalytic system may deactivate during photolysis, the decomposition of H_2A is the primary reason for the cease of hydrogen evolution after illumination.

3.5. Photocatalytic mechanism

It has been shown that the photocatalytic hydrogen evolution goes as follows: visible light absorption of the photosensitizer, formation of photo-generated charges, separation of electron–hole pair, and electron transfer. Fig. S23 shows the UV–vis diffuse reflectance spectra of the CdS NRs, the nickel complex, and the mixed complex **1**/CdS NR samples. The CdS NRs has a main absorption in the visible region with a band gap at ~2.34 eV. When mixing the nickel complex with CdS NRs, the band gap of CdS NRs remains unchanged. As shown in Fig. S23, the introduction of the nickel complex into CdS NRs results in a red shift of the absorption onset and reduction of Eg of CdS NRs, which obviously improves the range and ability of visible light absorption of CdS NRs. Based on XPS valence band spectra of CdS NRs (Fig. S24), a valance band (VB) of 1.81 eV is given. Combining with a band gap (2.34 eV) (Fig. S23), a conduction band (CB) of −0.53 eV is obtained.

To further look for the photocatalytic mechanism for hydrogen generation over the nickel complex modified CdS NRs, the photoluminescence (PL) spectra of the photocatalysts were provided, which are useful to answer the migration, transfer, and recombination processes of the photogenerated electron–hole pairs in CdS NRs, a photosensitizer [58]. As shown in Fig. S25, the PL data for the CdS NRs and complex **1**/CdS NRs, at the excitation wavelength of 450 nm, CdS NRs exhibits two emission peaks at 535 and 680 nm, respectively. However, the introduction of the nickel complex into CdS NRs leads to that the peak intensities of CdS NRs at both 535 and 680 nm decrease, showing a lower possibility of electron–hole pair recombination because of the fast electron transfer from CdS NRs to complex **1**. And the incorporation of the nickel complex on the CdS NRs surfaces in the reactive system acts as an electron acceptor, which efficiently traps photo-generated electrons and promotes their combination with H^+ to form H_2.

Further photolysis investigations were carried out to further characterize the photoinduced electron-transfer process. As shown in Fig. 9a, on laser excitation of the CdS NRs with light of 470 nm wavelength, no characteristic absorption signal could be detected. However, the introduction of complex **1** results in a strong absorption at around 588 nm (Fig. 9b). Although it is difficult to catch the intermediate species of the nickel complex, it is reasonable to speculate that a nickel (I) species is generated via the reduction of complex **1**, which was found in the reported samples [46,59,60].

To characterize the relationship between the electrocatalytic and photocatalytic performances, Mott–Schottky analysis were carried out, and the results were shown in Fig. S26. Mott–Schottky analysis gives a flat-band potential (E_{fb}) of −0.58 V versus Ag/AgCl (Fig. S26) [61]. The reductive potential of −0.24 V versus Ag/AgCl of complex **1** was taken from cyclic voltammogram (Fig. S6-inset in

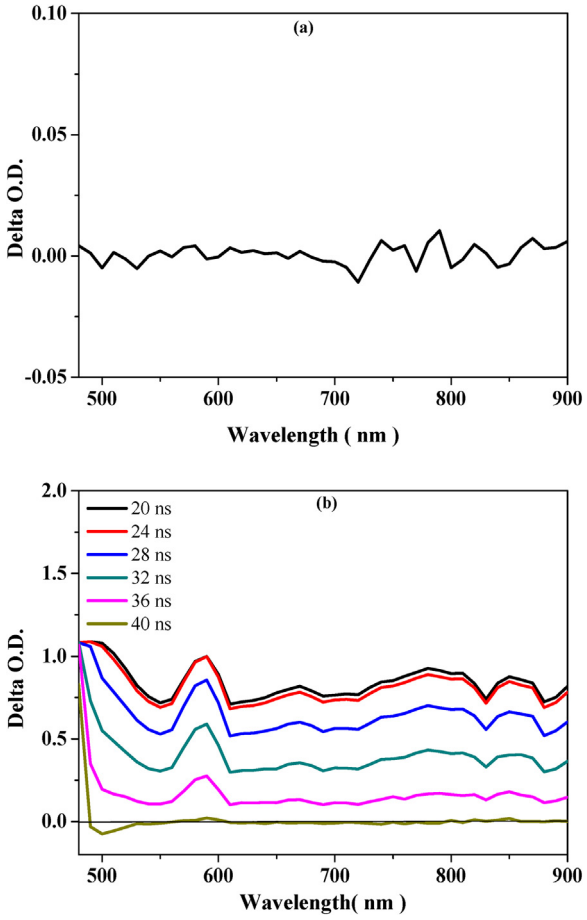

Fig. 9. (a) Transient absorption spectrum of CdS NRs in H_2O, on laser excitation using 470 nm light. (b) Transient absorption spectra of complex **1** and CdS NRs in H_2O, upon laser-pulsing (wavelength 470 nm).

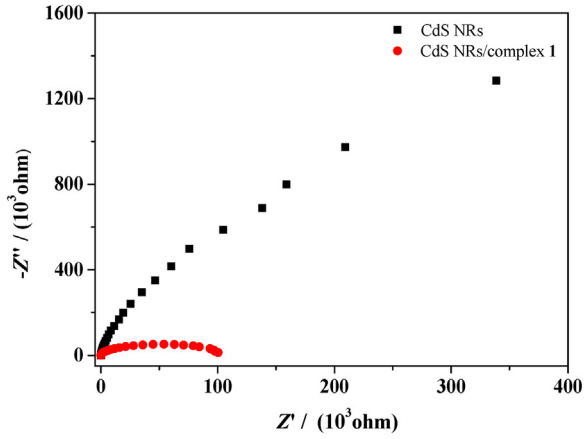

Fig. 10. Electrochemical impedance spectroscopy Nyquist plots of CdS NRs and complex **1**/CdS NRs with 0.010 M $K_3Fe(CN)_6/K_4Fe(CN)_6$ electrolyte in dark conditions.

the Supporting Information). The results implies that the electron transfer from the excited CdS NRs to the nickel complex is thermodynamically favorable. Moreover, electrochemical impedance spectroscopy was employed to investigate charge transfer properties and separation efficiency of photogenerated charge carriers. As shown in Fig. 10, compared with CdS NRs, the CdS NRs/complex **1** shows much smaller arc radius, representing a faster interfacial charge transfer and higher separation efficiency of photogener-

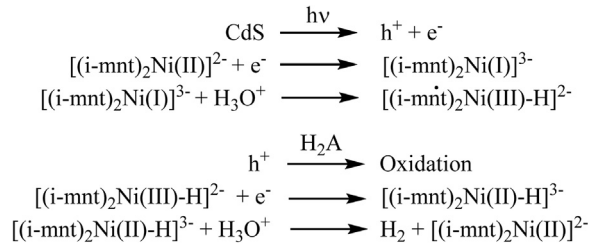

Scheme 3. A possible mechanism for H_2 production by the photocatalytic system.

ated charge carriers [62–64]. On the basis of the above observation, catalytic analysis and literature precedents [65–67], we put forward a possible mechanism for the photocatalytic H_2 production. As outlined in Scheme 3, the transfer of the photoexcited electron from the conduction band (CB) of CdS NRs to the nickel(II) ion of complex **1** affords the reduced nickel(I) species, a high reactive intermediate. The introduction of hydrogen proton yields the Ni^{III}-H species. Further addition of hydrogen proton to the Ni^{III}-H species gives dihydrogen, and regenerates the starting nickel complex **1**. Moreover, the photogenerated hole remaining in the CdS NSs is subsequently coupled with electrons come from H_2A, thus preventing the recombination of photogenerated charge carries and letting the continuous reactions.

4. Conclusion

We have designed successfully a new photocatalytic system for water reduction to dihydrogen. This system containing CdS NRs as a photosensitizer, the nickel complex as a cocatalyst, and H_2A as a sacrificial electron donor can work for about 100 h. Compared with CdS cluster as a precursor, CdS NR shows much better photocatalytic performance, indicating that the crystallinity of photosensitizer significantly effects the photocatalytic activity of the system. The studies show that CdS NRs and the nickel complex are stable and ascorbic acid is decomposed during light irradiation. These findings may offer a new chemical paradigm for the design of effective non-noble-metal catalysts for water reduction that is highly active in heterogeneous environments.

Acknowledgement

This work was supported by the National Science Foundation of China (No. 20971045, 21271073 and 21372088) and the Science and Technology Project (No. 2014A010105037) from Guangdong Science and Technology Department.

Appendix A. Supplementary data

Supplementary data associated with this article can be found, in the online version, at http://dx.doi.org/10.1016/j.apcatb.2017.07.034.

References

[1] M.G. Walter, E.L. Warren, J.R. McKone, S.W. Boettcher, Q.X. Mi, E.A. Santori, N.S. Lewis, Solar water splitting cells, Chem. Rev. 110 (2010) 6446–6473.
[2] A.J. Esswein, D.G. Nocera, Hydrogen production by molecular photocatalysis, Chem. Rev. 107 (2007) 4022–4047.
[3] T. Faunce, S. Styring, M.R. Wasielewski, G.W. Brudvig, A.W. Rutherford, J. Messinger, A.F. Lee, C.L. Hill, M. Fontecave, D.R. MacFarlane, Artificial photosynthesis as a frontier technology for energy sustainability, Energy Environ. Sci. 6 (2013) 1074–1076.
[4] J.H. Alstrum-Acevedo, M.K. Brennaman, T.J. Meyer, Chemical approaches to artificial photosynthesis. 2, Inorg. Chem. 44 (2005) 6802–6827.
[5] X.J. Lv, W.F. Fu, H.X. Chang, H. Zhang, J.S. Cheng, G.J. Zhang, Y. Song, C.Y. Hu, J.H. Li, Hydrogen evolution from water using semiconductor nanoparticle/graphene composite photocatalysts without noble metals, J. Mater. Chem. 22 (2012) 1539–1546.
[6] A.J. Bard, M.A. Fox, Artificial photosynthesis: solar splitting of water to hydrogen and oxygen, Acc. Chem. Res. 28 (1995) 141–145.
[7] J. Barber, Photosynthetic energy conversion: natural and artificial, Chem. Soc. Rev. 38 (2009) 185–196.
[8] W. Zhang, J. Hong, J. Zheng, Z. Huang, J. Zhou, R. Xu, Nickel-thiolate complex catalyst assembled in one step in water for solar H_2 production, J. Am. Chem. Soc. 133 (2011) 20680–20683.
[9] J.C. Fontecilla-Camps, A. Volbeda, C. Cavazza, Y. Nicolet, Structure/function relationships of [NiFe]- and [FeFe]-hydrogenases, Chem. Rev. 107 (2007) 4273–4303.
[10] P.M. Vignais, B. Billoud, Occurrence classification, and biological function of hydrogenases: an overview, Chem. Rev. 107 (2007) 4206–4272.
[11] M.P. McLaughlin, T.M. McCormick, R. Eisenberg, P.L. Holland, A stable molecular nickel catalyst for the homogeneous photogeneration of hydrogen in aqueous solution, Chem. Commun. 47 (2011) 7989–7991.
[12] L. Gan, T.L. Groy, P. Tarakeshwar, S.K.S. Mazinani, J. Shearer, V. Mujica, A.K. Jones, A nickel phosphine complex as a fast and efficient hydrogen production catalyst, J. Am. Chem. Soc. 137 (2015) 1109–1115.
[13] A. Das, Z.J. Han, W.W. Brennessel, P.L. Holland, R. Eisenberg, Nickel complexes for robust light-driven and electrocatalytic hydrogen production from water, ACS Catal. 5 (2015) 1397–1406.
[14] T. Lazarides, I.V. Sazanovich, A.J. Simaan, M.C. Kafentzi, M. Delor, Y. Mekmouche, B. Faure, M. Reglier, J.A. Weinstein, A.G. Coutsolelos, T. Tron, J. Am. Chem. Soc. 135 (2013) 3095–3103.
[15] W.R. McNamara, Z.J. Han, P.J. Alperin, W.W. Brennessel, P.L. Holland, R. Eisenberg, A cobalt-dithiolene complex for the photocatalytic and electrocatalytic reduction of protons, J. Am. Chem. Soc. 133 (2011) 15368–15371.
[16] E. Deponti, A. Luisa, M. Natali, E. Iengo, F. Scandola, Photoinduced hydrogen evolution by a pentapyridine cobalt complex: elucidating some mechanistic aspects, Dalton Trans. 43 (2014) 16345–16353.
[17] F. Gartner, A. Boddien, E. Barsch, K. Fumino, S. Losse, H. Junge, D. Hollmann, A. Bruckner, R. Ludwig, M. Beller, Photocatalytic hydrogen generation from water with iron carbonyl phosphine complexes: improved water reduction catalysts and mechanistic insights, Chem. Eur. J. 17 (2011) 6425–6436.
[18] B. Probst, C. Kolano, P. Hamm, R. Alberto, An efficient homogeneous intermolecular rhenium-based photocatalytic system for the production of H_2, Inorg. Chem. 48 (2009) 1836–1843.
[19] W.T. Eckenhoff, R. Eisenberg, Molecular systems for light driven hydrogen production, Dalton Trans. 41 (2012) 13004–13021.
[20] W.T. Eckenhoff, W.W. Brennessel, R. Eisenberg, Light-driven hydrogen production from aqueous protons using molybdenum catalysts, Inorg. Chem. 53 (2014) 9860–9869.
[21] A. Fujishima, K. Honda, Electrochemical photolysis of water at a semiconductor electrode, Nature 238 (1972) 37–38.
[22] Z.G. Zou, J.H. Ye, K. Sayama, H. Arakawa, Direct splitting of water under visible light irradiation with an oxide semiconductor photocatalyst, Nature 414 (2001) 625–627.
[23] I. Tsuji, H. Kato, H. Kobayashi, A. Kudo, Photocatalytic H_2 evolution reaction from aqueous solutions over band structure-controlled $(AgIn)_xZn_{2(1-x)}S_2$ solid solution photocatalysts with visible-light response and their surface nanostructures, J. Am. Chem. Soc. 126 (2004) 13406–13413.
[24] A. Kudo, Y. Miseki, Heterogeneous photocatalyst materials for water splitting, Chem. Soc. Rev. 38 (2009) 253–278.
[25] M.A. Gross, A. Reynal, J.R. Durrant, E. Reisner, Versatile photocatalytic systems for H_2 generation in water based on an efficient DuBois-Type nickel catalyst, J. Am. Chem. Soc. 136 (2014) 356–366.
[26] N.Z. Bao, L.M. Shen, T. Takata, K. Domen, Self-templated synthesis of nanoporous CdS nanostructures for highly efficient photocatalytic hydrogen production under visible light, Chem. Mater. 20 (2008) 110–117.
[27] H.J. Yan, J.H. Yang, G.J. Ma, G.P. Wu, X. Zong, Z.B. Lei, J.Y. Shi, C. Li, Visible-light-driven hydrogen production with extremely high quantum efficiency on Pt-PdS/CdS photocatalyst, J. Catal. 266 (2009) 165–168.
[28] L.A. Silva, S.Y. Ryu, J. Choi, W. Choi, M.R. Hoffmann, Photocatalytic hydrogen production with visible light over Pt-interlinked hybrid composites of cubic-phase and hexagonal-phase CdS, J. Phys. Chem. C 112 (2008) 12069–12073.
[29] Y.X. Li, G.F. Ma, S.Q. Peng, G.X. Lu, S.B. Li, Photocatalytic H_2 evolution over basic zincoxysulfide $(ZnS_{1-x-0.5y}O_x(OH)_y)$ under visible light irradiation, Appl. Catal. A: Gen. 363 (2009) 180–187.
[30] T. Simon, N. Bouchonville, M.J. Berr, A. Vaneski, A. Adrovic, D. Volbers, R. Wyrwich, M. Doblinger, A.S. Susha, A.L. Rogach, F. Jackel, J.K. Stolarczyk, J. Feldmann, Redox shuttle mechanism enhances photocatalytic H_2 generation on Ni-decorated CdS nanorods, Nat. Mater. 13 (2014) 1013–1018.
[31] K. Wu, Y. Du, H. Tang, Z. Chen, T. Lian, Efficient extraction of trapped holes from colloidal CdS nanorods, J. Am. Chem. Soc. 137 (2015) 10224–10230.
[32] M.B. Wilker, K.E. Shinopoulos, K.A. Brown, D.W. Mulder, P.W. King, G. Dukovic, Electron transfer kinetics in CdS nanorod-[FeFe]-hydrogenase complexes and implications for photochemical H_2 generation, J. Am. Chem. Soc. 136 (2014) 4316–4324.
[33] J. Chen, X. Wu, L. Yin, B. Li, X. Hong, Z. Fan, B. Chen, C. Xue, H. Zhang, One-pot synthesis of CdS nanocrystals hybridized with single-layer transition-metal dichalcogenide nanosheets for efficient photocatalytic hydrogen evolution, Angew. Chem. 127 (2015) 1226–1230.

[34] R. Marschall, Semiconductor composites: strategies for enhancing charge carrier separation to improve photocatalytic activity, Adv. Funct. Mater. 24 (2014) 2421–2440.
[35] F.Y. Wen, C. Li, Hybrid artificial photosynthetic systems comprising semiconductors as light harvesters and biomimetic complexes as molecular cocatalysts, Acc. Chem. Res. 46 (2013) 2355–2364.
[36] Q. Li, B. Guo, J. Yu, J. Ran, B. Zhang, H. Yan, J.R. Gong, Highly efficient visible-light-driven photocatalytic hydrogen production of CdS-cluster-decorated graphene nanosheets, J. Am. Chem. Soc. 133 (2011) 10878–10884.
[37] X.X. Zouc, Y. Zhang, Noble metal-free hydrogen evolution catalysts for water splitting, Chem. Soc. Rev. 44 (2015) 5148–5180.
[38] F.Y. Wen, J.H. Yang, X. Zong, B.J. Ma, D.G. Wang, C. Li, Photocatalytic H_2 production on hybrid catalyst system composed of inorganic semiconductor and cobaloximes catalysts, J. Catal. 281 (2011) 318–324.
[39] X. Yin, L. Li, W. Jiang, Y. Zhang, X. Zhang, L. Wan, J. Hu, MoS_2/CdS nanosheets-on-nanorod heterostructure for highly efficient photocatalytic H_2 generation under visible light irradiation, ACS Appl. Mater. Interfaces 8 (2016) 15258–15266.
[40] H. Chen, Z. Sun, S. Ye, D. Lu, P. Du, Molecular cobalt-salen complexes as novel cocatalysts for highly efficient photocatalytic hydrogen production over a CdS nanorod photosensitizer under visible light, J. Mater. Chem. A 3 (2015) 15729–15737.
[41] Y. Xu, X. Yin, Y. Huang, P. Du, B. Zhang, Hydrogen production on a hybrid photocatalytic system composed of ultrathin CdS nanosheets and a molecular nickel complex, Chem. Eur. J. 21 (2015) 4571–4575.
[42] S.B. Bulgarevich, D.V. Bren, D.Y. Movshovic, P. Finocchiaro, S. Failla, Conformational investigation of N-aralkylpyridinium ions by Cotton-Mouten effect method, J. Mol. Struct. 317 (1994) 147–155.
[43] C. Feng, X. Li, Y. Hou, C. Ni, Bis[1-benzyl-4-(dimethylamino)-pyridinium] bis(2, 2-dicyanoethylene-1, 1-dithiolato-(^{2}S, S')nickelate(II), Acta Cryst. E63 (2007) m1762.
[44] J.S. Jang, U.A. Joshi, J.S. Lee, Solvothermal synthesis of CdS anowires for photocatalytic hydrogen and electricity production, J. Phys. Chem. C 111 (2007) 13280–13287.
[45] E.S. Rountree, J.L. Dempsey, Potential-dependent electrocatalytic pathways: controlling reactivity with pK_a for mechanistic investigation of a nickel-based hydrogen evolution catalyst, J. Am. Chem. Soc. 137 (2015) 13371–13380.
[46] Z. Han, L. Shen, W.W. Brennessel, P.L. Holland, R. Eisenberg, Nickel pyridinethiolate complexes as catalysts for the light-driven production of hydrogen from aqueous solutions in noble-metal-free systems, J. Am. Chem. Soc. 135 (2013) 14659–14669.
[47] Y.-X. Zhang, L.-Z. Tang, Y.-F. Deng, S.-Z. Zhan, Synthesis and electrocatalytic function for hydrogen generation of cobalt and nickel complexes supported by phenylenediamine ligand, Inorg. Chem. Commun. 72 (2016) 100–104.
[48] G.A.N. Felton, R.S. Glass, D.L. Lichtenberger, D.H. Evans, Iron-only hydrogenase mimics. Thermodynamic aspects of the use of electrochemistry to evaluate catalytic efficiency for hydrogen generation, Inorg. Chem. 45 (2006) 9181–9184.
[49] T. Fang, L.-Z. Fu, L.L. Zhou, S.-Z. Zhan, S. Chen, Electrochemical-driven water reduction catalyzed by a water soluble cobalt(III) complex with Schiff base ligand, Electrochim. Acta 178 (2015) 368–373.
[50] R.S. Nichloson, I. Shain, Theory of stationary electrode polarography. Single scan and cyclic methods applied to reversible irreversible, and kinetic systems, Anal. Chem. 36 (1964) 706–723.
[51] H.I. Karunadasa, C.J. Chang, J.R. Long, A molecular molybdenum-oxo catalyst for generating hydrogen from water, Nature 464 (2010) 1329–1333.
[52] W.T. Lee, S.B. Munoz III, D.A. Dickie, J.M. Smith, Ligand modification transforms a catalase mimic into a water oxidation catalyst, Angew. Chem. Int. Ed. 53 (2014) 9856–9859.
[53] W.M. Singh, T. Baine, S. Kudo, S. Tian, X.A.N. Ma, H. Zhou, N.J. DeYonker, T.C. Pham, J.C. Bollinger, D.L. Baker, B. Yan, C.E. Webster, X. Zhao, Electrocatalytic and photocatalytic hydrogen production in aqueous solution by a molecular cobalt complex, Angew. Chem. Int. Ed. 51 (2012) 5941–5944.
[54] D.J. Martin, K.P. Qiu, S.A. Shevlin, A.D. Handoko, X.W. Chen, Z.X. Guo, J.W. Tang, Highly efficient photocatalytic H_2 evolution from water using visible light and structure-controlled graphitic carbon nitride, Angew. Chem. Int. Ed. 53 (2014) 9240–9245.
[55] Y.T. Chen, J.B. Ding, Y. Guo, L.B. Kong, H.L. Li, A facile route to preparation of CdS nanorods, Mater. Chem. Phys. 77 (2003) 734–737.
[56] Z.H. Yang, H.B. Chu, Z. Jin, W.W. Zhou, Y. Li, Preparation and properties of CdS/Au composite nanorods and hollow Au tubes, Chin. Sci. Bull. 55 (2010) 921–926.
[57] S.H. Hsu, S.F. Hung, S.H. Chien, CdS sensitized vertically aligned single crystal TiO_2 nanorods on transparent conducting glass with improved solar cell efficiency and stability using ZnS passivation layer, J. Power Sources 233 (2013) 236–243.
[58] C. Han, L. Ge, C. Chen, Y. Li, X. Xiao, Y. Zhang, L. Guo, Novel visible light induced Co_3O_4-g-C_3N_4 heterojunction photocatalysts for efficient degradation of methyl orange, Appl. Catal. B 147 (2014) 546–553.
[59] W. Zhang, J. Hong, J. Zheng, Z. Huang, J. Zhou, R. Xu, Nickel?thiolate complex catalyst assembled in one step in water for solar H_2 production, J. Am. Chem. Soc. 133 (2011) 20680–20683.
[60] M.P. McLaughlin, T.M. McCormick, R. Eisenberg, P. Holland, A stable molecular nickel catalyst for the homogeneous photogeneration of hydrogen in aqueous solution, Chem. Commun. 47 (2011) 7989–7991.
[61] Y. Liu, Y.-X. Yu, W.-D. Zhang, MoS_2/CdS heterojunction with high photoelectrochemical activity for H_2 evolution under visible light: the role of MoS_2, J. Phys. Chem. C 117 (2013) 12949–12957.
[62] L.-W. Zhang, H.-B. Fu, Y.-F. Zhu, Efficient TiO_2 photocatalysts from surface hybridization of TiO_2 particles with graphite-like carbon, Adv. Funct. Mater. 18 (2008) 2180–2189.
[63] Y.-X. Yu, W.-X. Ouyang, Z.-T. Liao, B.-B. Du, W.-D. Zhang, Construction of ZnO/ZnS/CdS/$CuInS_2$ core-shell nanowire arrays via ion exchange: p-n junction photoanode with enhanced photoelectrochemical activity under visible light, ACS Appl. Mater. Interfaces 6 (2014) 8467–8474.
[64] L. Jia, D.-H. Wang, Y.-X. Huang, A.-W. Xu, H.-Q. Yu, Highly durable N-doped graphene/CdS nanocomposites with enhanced photocatalytic hydrogen evolution from water under visible light irradiation, J. Phys. Chem. C 115 (2011) 11466–11473.
[65] W. Zhang, J. Hong, J. Zheng, Z. Huang, J. Zhou, R. Xu, Nickel-thiolate complex catalyst assembled in one step in water for solar H_2 production, J. Am. Chem. Soc. 133 (2011) 20680–20683.
[66] Z. Han, L. Shen, W.W. Brennessel, P.L. Holland, R. Eisenberg, Nickel pyridinethiolate complexes as catalysts for the light-driven production of hydrogen from aqueous solutions in noble-metal-free systems, J. Am. Chem. Soc. 135 (2013) 14659–14669.
[67] M.P. McLaughlin, T.M. McCormick, R. Eisenberg, P. Holland, A stable molecular nickel catalyst for the homogeneous photogeneration of hydrogen in aqueous solution, Chem. Commun. 47 (2011) 7989–7991.